# Clustered Nanocarriers: The Effect of Size on the Clustering of CCMV Virus-Like Particles With Soft Macromolecules

Martijn Verwegen, Jeroen J. L. M. Cornelissen*

Virus-like particles (VLP) could enable a wide variety of biomedical applications in therapy, drug delivery, and imaging. They are biocompatible and can be self-assembled into larger structured materials for additional functionality and potentially better biodistribution, which is still a challenging aspect. Here we investigate the role of the VLPs size and resulting Caspar Klug symmetry in forming clusters out of these building blocks, showing that the onset point for clustering is determined by steric considerations of the binding site and binding agent. The clustering is independent of cargo and the data suggests that rotational symmetry in the $T = 3$ capsid allows for hexagonal close packed structures, whereas the $T = 1$ capsid that lacks a six-fold and twofold rotational axis does not show such organization.
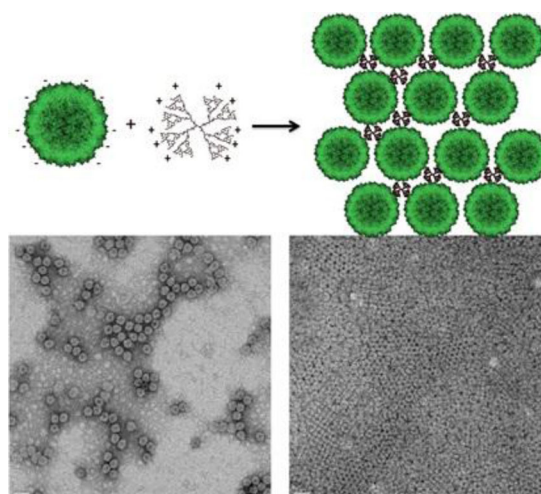
1. Introduction

1.1. Scientific Scope

Individual nanoparticles are well established in having a wide variety of nano-medicinal applications in therapy, drug delivery, and imaging.[1a] Challenges remain in the toxicity, ability to overcome biological barriers and biodistribution of many of these nanoparticles, resulting from their low biocompatibility and their small size.[2] Organized peptide based nanomaterials, such as virus-like particles (VLPs), have the potential to address these challenges by providing a biocompatible scaffold and enabling control over the shape and size of the structures. Furthermore, these organized materials could be used to combine different nanoparticles with various properties and provide a structural role. This could potentially enable the above mentioned biomedical applications or even cell adhesion and tissue regeneration.

All of this, however, could benefit from an ordered structure and large-scale combination of different nanoparticles to achieve the desired result. The degree of organization and scale are also where the principle challenges in this field lie, as due to the multitude of nanoscale forces, so far, no single technique can cover both challenges for different particles.[3] Therefore, we believe in simplifying the problem by limiting the number of different particles that need to be organized by using virus protein shells to first encapsulate the desired nanoparticle before forming the assembly.

Dr. M. Verwegen, Prof. J. J. L. M. Cornelissen
Laboratory for Biomolecular Nanotechnology, MESA+ Institute for Nanotechnology, University of Twente, P.O. Box 217, 7500 AE, Enschede, The Netherlands
E-mail: J.J.L.M.Cornelissen@utwente.nl

1.2. Nano-Assemblies of Virus-Like Particles

Viruses and VLPs have seen extensive use as nanocarriers in biomedicine and are by nature biocompatible, thus covering the first challenge.[1b] The application of VLPs in materials science, therefore, is an emerging area of interest,[4,5] Furthermore, many techniques exist to form assemblies from viruses and VLPs, from protein crystallization techniques,[6a] modification[7] to using covalent linkers[8] and electrostatics.[9] The first two, however, are techniques that require a great deal of time and effort as they rely on slow crystallization processes or layer-by-layer material deposition. Electrostatic assembly can, however, be achieved in solution rather than on a surface or through layer-by-layer assembly by using cationic polyelectrolytes.[10a] This opens up the possibility of rapidly assembling different materials contained inside the capsid into large-scale organized structures. Not all VLPs with encapsulated particles confirm to the native size and thus symmetry, which, despite using the same protein, will affect their ability to cluster.[6b]

1.3. Size and Symmetry in Virus Capsids

Formation of VLP clusters by electrostatics is affected by virus Caspar Klug symmetry structures. Recent experimental studies and theoretical simulations confirm that symmetrically placed patches of electrostatic charge aid and guide the clustering of viruses.[11] However, under Caspar Klug symmetry laws, the virus proteins can also form different sized VLPs that do not have the same symmetry as the native virus.[12] Therefore, the symmetrical charge distribution can differ in different sized VLPs, even though the overall charge density is similar as the same proteins are used. Clustering could thus be controlled by controlling the capsid size and resulting symmetry.

Coat proteins (CP) can fold into these different symmetrical architectures following the size of a presented template. This allows for the encapsulation of functional materials into a variety of capsid sizes and resulting symmetries. Spherical symmetry sizes follow Caspar Klug symmetry laws, with stable capsid shells being formed at discreet intervals, governed by the triangulation (T) number, and containing 60*T proteins.[a] Cowpea Chlorotic Mottle Virus (CCMV) makes an excellent model system, as its CP have been shown to adopt $T = 1$, pseudo '$T = 2$', and $T = 3$ as well as rod-like symmetries using the right template.[13] Furthermore the clustering of the $T = 3$ symmetrical structure is well studied by Kostiainen et al.[10a][14] In this experimental study we have combined

CCMV CP with anionic templates to study the difference in clustering behavior between $T = 1$, $T = 3$, and mixed VLPs.

1.4. Content

In this study, the clustering of $T = 1$ and $T = 3$ CCMV based VLPs is studied and analyzed to understand the effect of different size and symmetry VLPs on cluster formation. First, the formation of the $T = 1$ and $T = 3$ VLPs according to procedures adapted from literature and earlier work is briefly described with emphasis on the relevant differences between the VLPs. Subsequently, the effect of the ionic strength, polymer shape, VLP core and clustering dynamics are presented to further understand these systems. This interplay between ionic strength and symmetry is shown to be a dominant force in the clustering of these particles. Finally, a comparison to a model that shows the different electrostatic binding pockets for the $T = 1$ and $T = 3$ CCMV capsids is used to explain this behavior.

2. Results and Discussion

2.1. Formation of $T = 1$ and $T = 3$ VLPs

In order to study the clustering of different sized VLPs, several model VLPs are selected and synthesized using known procedures. In this, the native $T = 3$ CCMV, having a resolved crystal structure and known clustering properties with different soft macromolecules, serves as the model for $T = 3$ sized capsids.[10b] To compliment this, two known $T = 1$ VLPs, CCMV with a 70 kDa polystyrene sulfonate core (CPSS) and CCMV with a 7 nm gold nanoparticle core (CAu7T), are synthesized following known encapsulation procedures (Figure 1).[15] In brief, these procedures are detailed below, with emphasis given to the clustering-relevant properties of these different VLPs.

The native $T = 3$ capsid of CCMV can be extracted from infected cowpea plants and subsequently disassembled into 90 protein dimers by removing the RNA, both following established procedures.[16] These dimers can be reassembled into well-studied $T = 1$ capsid VLPs by encapsulating negatively charged gold nanoparticles (AuNP) or polystyrene sulfonate (PSS). The efficient formation of $T = 1$ capsids using PSS, as described by Sikkema et al.,[15] requires a precise ratio between polymer and protein, such that for each protein monomer 40 sulfonate groups are available. Encapsulation of AuNP is done by adding an excess of CP to solution of 7 nm AuNP, taking care to keep the NaCl concentration around 0.1 M.

The resulting VLPs were characterized using FPLC, DLS, agarose gel electrophoresis (Figure 2), and TEM (Figure 3) to check for successful VLP formation and confirm that their size correlates with either a $T = 3$ or $T = 1$ VLP. The FPLC size

---

[a]Note that not all T numbers form stable, symmetrical capsids shells, as explained by Caspar and Klug.[9]

Materials
Views
www.MaterialsViews.com

Macromol. Biosci. **2015,** *15,* 98–110
© 2014 WILEY-VCH Verlag GmbH & Co. KGaA, Weinheim
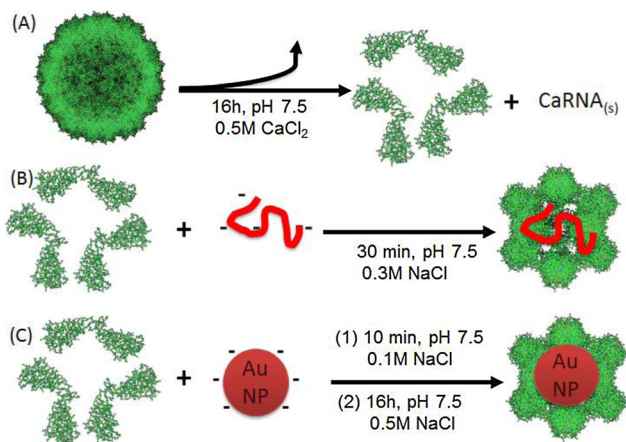
Macromolecular
Journals

99

Figure 1. Scheme showing; a) the disassembly of the $T = 3$ native CCMV using precipitation of RNA by calcium at pH 7.5; b) encapsulation of 70 kDa polystyrene sulfonate by CCMV coat protein to form a $T = 1$ VLP; c) encapsulation of tannic acid stabilized 7 nm gold nanoparticles to form a $T = 1$ VLP.

exclusion chromatograms show the expected elution volumes of $V = 10.3$ ml for CCMV ($T = 3$), $V = 12.7$ ml for CPSS ($T = 1$) and $V = 2.3$ ml for CAu7T ($T = 1$) with any leftover CP residue eluting at $V = 18$ ml.[b] The DLS and TEM confirm relatively monodisperse particles have formed, with an approximate of 28 nm for the CCMV $T = 3$ particle and 18 nm for both the CPSS and CAu7T $T = 1$ VLPs. Finally, agarose gel electrophoresis shows a uniform electrophoretic mobility, and thus charge/mass ratio, for all VLP, as expected from particles that have the same type of proteins forming the outer shell.

UV–Vis spectroscopy was used to further characterize the VLPs (Figure 2**c**). The native CCMV is known to have a large characteristic UV–Vis absorption at $\lambda = 260$ nm due to the presence of RNA ($\varepsilon_{260} = 2.78 \times 10^7 \, \mathrm{M^{-1} \, cm^{-1}}$) with little contribution of the protein absorbance peak at $\lambda = 280$ nm ($\varepsilon_{280} = 2.41 \times 10^4 \, \mathrm{M^{-1} \, cm^{-1}}$), which is confirmed for the isolated CCMV $T = 3$ particles.[17] After the encapsulation of PSS or Au7T the characteristic $\lambda = 260$ nm peak is lost, instead the CPSS shows a shift to $\lambda = 280$ nm and the CAu7T VLPs show the characteristic gold plasmon absorbance peak at $\lambda = 520$ nm. Due to their spectral overlap the relative absorptions of the CCMV-CP and PSS at $\lambda = 260$ nm and $\lambda = 80$ nm ($\varepsilon_{260,\mathrm{PSS}} = 2.17 \times 10^6 \, \mathrm{M^{-1} \, cm^{-1}}$, $\varepsilon_{280,\mathrm{PSS}} = 4.96 \times 10^5 \, \mathrm{M^{-1} \, cm^{-1}}$) have been used to calculate the concentrations of CPSS. For CAu7T the gold plasmon peak at $\lambda = 506$ nm (for 7 nm AuNP, $\varepsilon_{506, 7\,\mathrm{nm\,AuNP}} = 2.73 \times 10^7 \, \mathrm{M^{-1}}$ $\mathrm{cm^{-1}}$) is used to determine particle concentration after

purification as the change in the plasmon peak is negligible.[18]

2.2. Ionic Strength Dependence of Clustering different Sized VLPs

When examining the interaction of particles and polymers through electrostatic forces, the ions in solution must be considered. These can screen charges and lead to an effective reduction of interaction strength. By tuning this interaction strength, the speed of clustering can be tuned from rapid aggregation with little order to slow formation of periodic crystals or even an altogether stop of the clustering. The Debye screening length (κ), see Equation (1), the distance at which electrostatic interactions become meaningful, is indicative of this effect and is given by:[19]

$$\kappa^{-1} = \sqrt{\frac{\varepsilon_0 \varepsilon_r k_b T}{e^2 \sum_i c_i z_i^2}} \qquad (1)$$

Clusters of CCMV and CPSS are formed by adding an increasing concentration of poly-λ-lysine (PLL) to a fixed concentration of VLPs (Figure 4). In an ideal system the minimum amount of polymer needed to cluster the VLP is such that all electrostatic binding sites on one VLP share one polymer with one binding site on another VLP. These binding sites are known to occur on the threefold axis, with the $T = 3$ CCMV thus having 60 such binding sites, which, assuming the $T = 1$ VLPs have a similar binding site, means 20 such binding sites on the $T = 1$ VLPS. Significant variation from the amount of polymer being needed per two binding sites (i.e., one) indicates that the anionic binding sites of the system are screened by the ionic strength of the solution.

The formation of clusters of these VLPs and PLL is followed by DLS at different ionic strengths to characterize the dependence on the ionic strength. Buffered solutions with 150 mM NaCl (165 mM Na$^+$, so $\kappa \approx 0.8$ nm), 50 mM NaCl (65 mM Na$^+$, so $\kappa \approx 1.2$ nm) and 0 mM NaCl (15 mM Na$^+$, so $\kappa \approx 2.5$ nm) show varying onset points for the formation of polymer-VLP clusters. In this, we consider the onset point of clustering, an indication of how many polymers are needed per binding site, to be the point at which the DLS intensity signal indicates the presence of particles significantly larger than the capsid used. Two things become immediately apparent from the DLS results: firstly, the onset point for clustering is dependent on the ionic strength as expected, and, secondly, the two capsids behave different as the concentration of NaCl increases.

The 60 binding sites of the $T = 3$ capsid and 20 of the $T = 1$ capsid allow for 30 or 10 polymers respectively to interact with the capsid assuming two binding sites per polymer, an effective ratio of 6 proteins per polymer regardless of symmetry. Thus 50 µg/ml of protein (Mw$_{\mathrm{of\,protein}} = 20$ kDa, 2.5 mM) would require 3.96 µg/ml of PLL (Mw$_{\mathrm{average}} = 9500$

---

[b]The small difference in elution volume, $\Delta V = 0.4$, between CPSS and CAu7T VLPs can be attributed to the hard AuNP encapsulated in the CAu7T VLP, making this VLP slightly less compressible and malleable in the FPLC column compared to soft macromolecule (PSS) cored VLP.
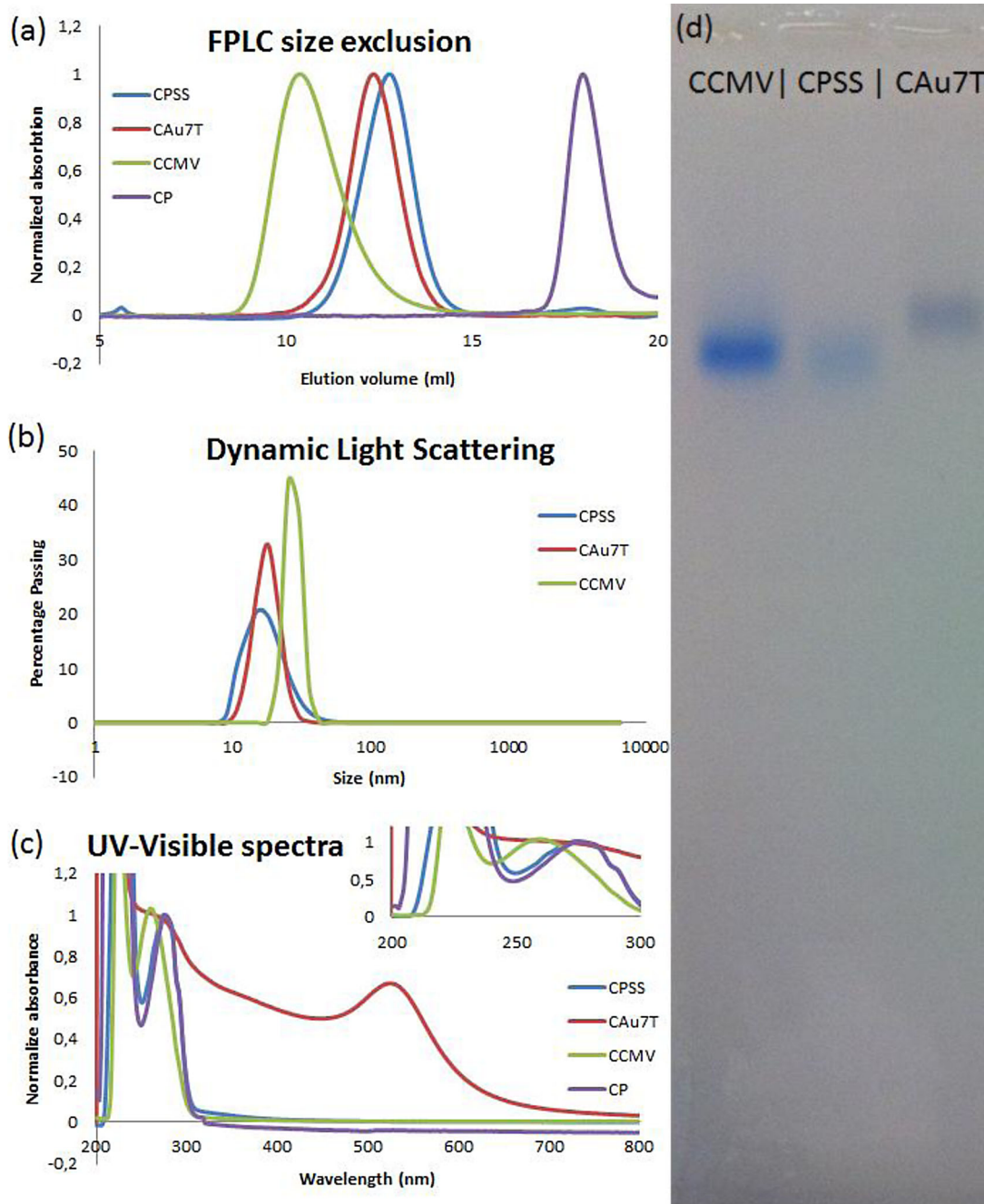
Figure 2. a) FPLC size exclusion chromatograms at λ = 280 nm absorption for CCMV, CCMV CP, CPSS, and CAu7T. b) Dynamic light scattering plots for CCMV, CPSS, and CAu7T. c) Normalized UV–Visible spectra for CPSS, CAu7T, CCMV, and CCMV CP, with inset showing an expansion of the range relevant for RNA, PSS, and protein absorptions. d) Agarose gel electrophoresis of $T = 3$ CCMV (left), $T = 1$ CPSS (middle), and $T = 1$ CCMV AuNP (right).

kDa, 0.417 mM) to allow for an optimal interaction assuming no competing ions shield the electrostatic binding sites. At first glance the DLS data (Figure 5) shows that for $T = 3$ capsids this holds at 0 and 50 mM, but the ionic strength is too high for optimal cluster formation at 150 mM. For the $T = 1$ particles this seems to require a

further analysis as their clustering already seems hindered from 50 mM NaCl onwards, even though the surface charge density of both $T = 3$ and $T = 1$ VLPs should be similar.

At 0 mM NaCl the number of competing ions is lowest and the DLS data (Figure 5) indeed shows an onset point of clustering between 1 and 5 μg/ml of PLL for both the $T = 1$

Materials
Views
www.MaterialsViews.com

Macromol. Biosci. **2015**, 15, 98–110
© 2014 WILEY-VCH Verlag GmbH & Co. KGaA, Weinheim
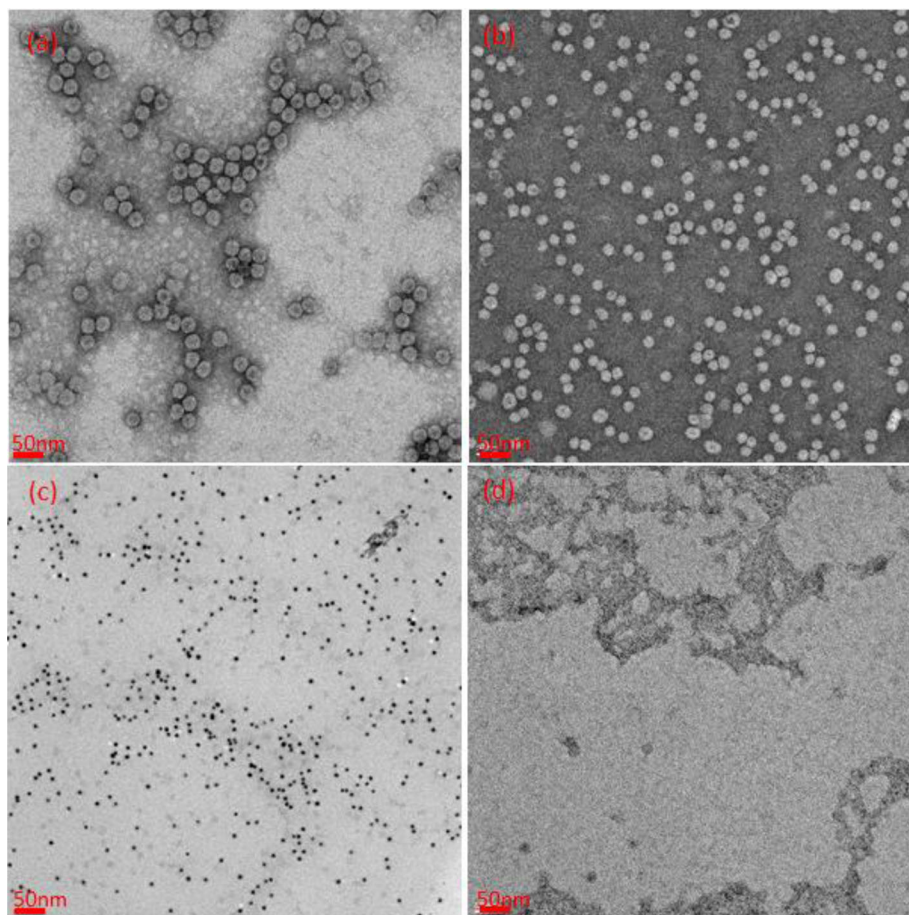
Macromolecular
Journals

101

Figure 3. TEM images of a) virus particles (CCMV), b) $T = 1$ polymer cored virus capsids (CPSS), c) gold cored $T = 1$ virus capsids (CAu7T), d) disassembled CCMV coat protein (CP).

and the $T = 3$ capsids. TEM micrographs taken at 5 µg/ml of PLL and 0 mM NaCl (Figure 6**a and c**), however, do not show any signs of organized structures. In fact, the $T = 3$ capsids form a random colloidal assembly (Figure 6**a**), whilst the
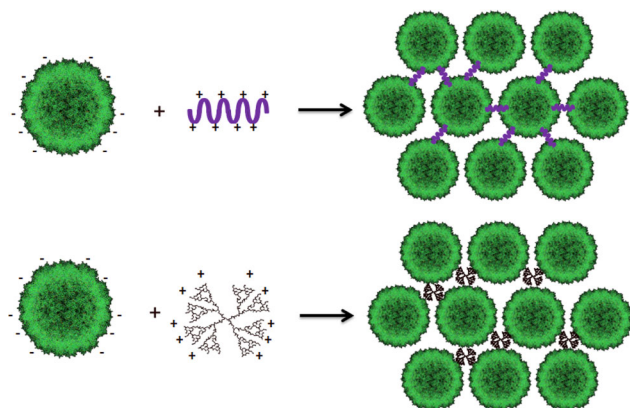

Figure 4. Schematic representation of VLP clustering with (top) linear poly-λ-lysine (PLL) and (bottom) spherical PAMAM G-3 dendrimers.

$T = 1$ capsids are packaged closely but with a clear fluctuation in the density of capsid particles (Figure 6**c**). It is likely that these assemblies are the result of extremely rapid aggregation of the particles upon exposure to the polymer possibly leading to kinetically trapped states.

As stated, at [NaCl] > 50 mM there is a clear difference between the $T = 1$ and $T = 3$ VLPs clustering behavior, as evident from the DLS data (Figure 5). Most importantly, the $T = 3$ particles seem to still be able to form clusters near the calculated 3.94 µg/ml calculated for optimal interaction. Furthermore TEM micrographs for $T = 3$ capsids cluster with 5 µg/ml of PLL (Figure 6**b**), close to this optimal interaction, show the formation of organized nanostructures. Unlike the $T = 3$ VLPs, the $T = 1$ VLPs do not show this desired organization and clustering behavior, and instead require concentrations of 25 µg/ml PLL (2.63 mM) or greater before clustering is initiated. This effectively means that an average of more than 1 polymer per protein, or 3 polymers per binding site, is needed before clustering starts. This is confirmed by TEM micrographs (Figure 6**d**), which show loose strips of protein cages not unlike those, found without
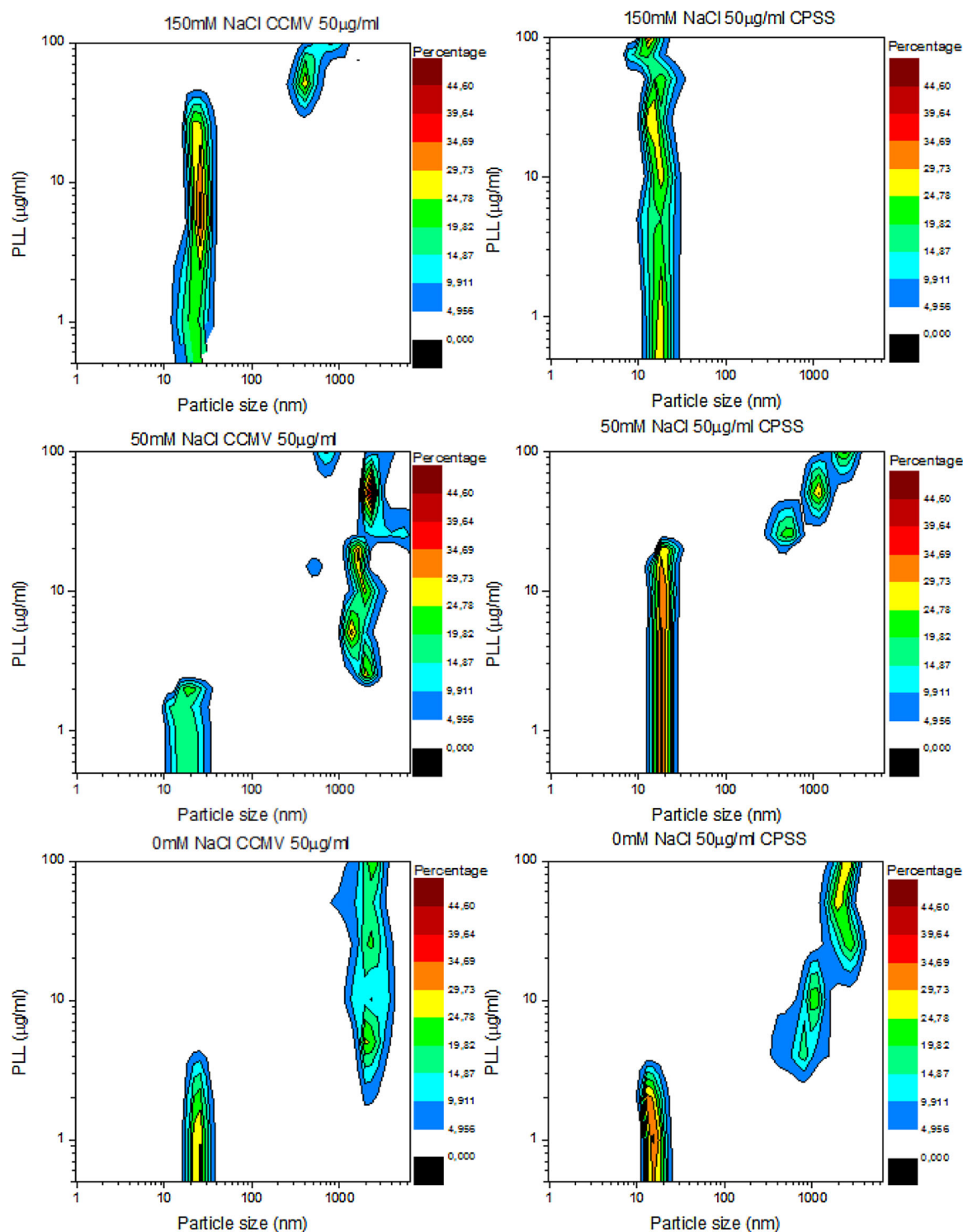
102

www.MaterialsViews.com

Figure 5. Dynamic light scattering intensity plots of 50 µg/ml (left) $T = 3$ virus particles (CCMV) and (right) $T = 1$ polymer cored virus capsids (CPSS) at (top to bottom) 150, 50, and 0 mM of NaCl. Note that a fictive 1×10^{-6} µg/ml concentration of PLL was used to plot the measurements for the capsid stock capsid solutions.
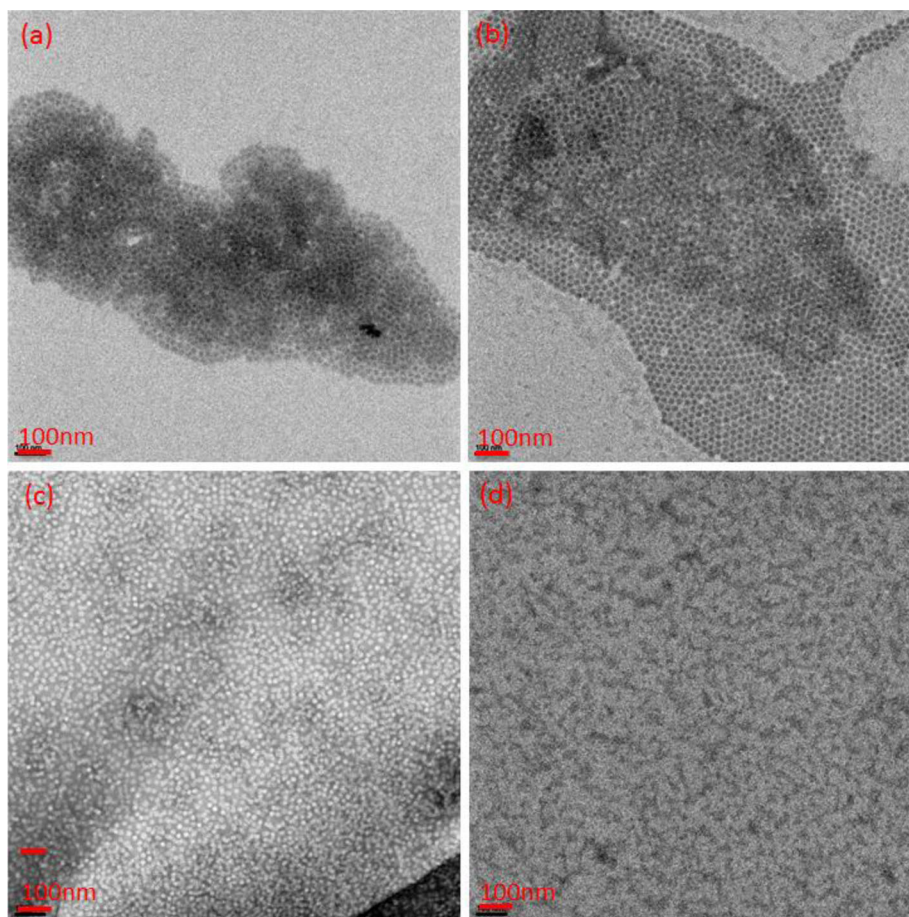
Makrials Views
www.MaterialsViews.com

Macromol. Biosci. **2015,** *15,* 98–110
© 2014 WILEY-VCH Verlag GmbH & Co. KGaA, Weinheim

Macromolecular
Journals

103

Figure 6. Transmission electron micrographs of 50 μg/ml VLPs, protein mass only, and 5 μg/ml of PLL of a) $T=3$ CCMV VLPs at 0 mM NaCl, b) $T=3$ CCMV VLPs at 50 mM NaCl, c) $T=1$ CPSS VLPs at 0 mM NaCl, and d) $T=1$ CPSS VLPs at 50 mM NaCl.

the presence of a clustering polymer. It should, however, be noted that the quality of the staining of these $T=1$ samples is poor, which, despite similar conditions to the other samples and several attempts, did not allow for better contrast. This is likely caused by the PLL, which screens the carboxylic acid groups in the binding sites on the surface from the uranyl acetate staining, resulting in a reduced level of staining and thus contrast.

2.3. Binding of Poly-λ-Lysine by the $T=1$ Capsid

The differences in the binding of PLL by the $T=1$ CPSS compared to the $T=3$ CCMV requires further examination. Therefore, the DLS and TEM results are compared to agarose gel electrophoresis and models for the $T=1$ and $T=3$ VLP capsid, to investigate the nature of the binding between the $T=1$ CPSS VLP and PLL. As stated, the effect of ionic strength on this binding is more pronounced in the $T=1$ CPSS VLP compared to the $T=3$ VLP, which we feel can be attributed to the capsid symmetry itself and not to the change from an

RNA type core to a PSS type core. Both are, after all, relatively soft macromolecules and PSS is a well-studied RNA mimic for virus assembly.[15] As seen in the structural model (Figure 7), the relevant change between the $T=1$ and $T=3$ symmetrical structures lies in a structural change of the negatively charged electrostatic binding site near the threefold axis, which could explain the difference in binding.

The VLP binding site (Figure 7) changes from a pocket, formed by two proteins from two different hexamers and one from a pentamer, for $T=3$ VLPs, to a 2 nm groove formed by three proteins derived solely from three different pentamers for $T=1$ VLPs. Assuming the binding site has in fact changed as suggested; two key parameters can change in the protein shell electrostatics, namely the surface charge density and the charge distribution. Agarose gel electrophoresis (Figure 2**c**) confirms that the overall surface charge to mass ratio does not change from the $T=3$ to the $T=1$ VLPs, as both capsids show an equal electrophoretic mobility on the gel. On the other hand, the above model
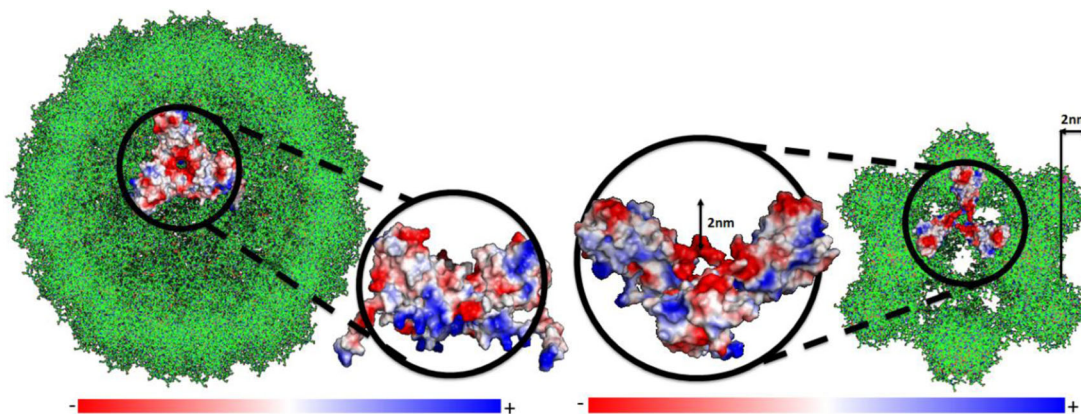
Figure 7. To scale reconstruction of $T = 3$ (left) and $T = 1$ (right) symmetry capsids with electrostatic potential map of the 3-fold symmetry axis for both symmetries.

shows a change in the distribution of charge within each binding site, which could explain the effect of the ionic strength contribution to the electrostatic clustering. After all starting at 50 mM NaCl ionic strength the Debye screening length is comparable to the depth of the groove, ensuring that charges inside the groove have little interaction with charge outside. At 0 mM NaCl there is little charge screening allowing polymers to fully interact with neighboring particles, whereas at 150 mM all interaction outside of the groove is quenched.

This is supported by agarose gel electrophoresis analysis of the $T = 1$ and $T = 3$ VLP clusters at increasing concentration of PLL (Figure 8). In this, $T = 3$ CCMV clusters show only two possible protein bands, whilst the $T = 1$ CPSS clusters show three distinct protein bands. The top band/smear for both the $T = 3$ CCMV and $T = 1$ CPSS clusters can be attributed to clusters of particles slowly breaking up under the applied electric field. The lower bands for the $T = 3$ CCMV clusters slowly decrease in electrophoretic mobility as the PLL concentration increases, an effect likely caused by reversible interaction with PLL. Unlike the $T = 3$ clusters, the lowest band for the $T = 1$ particles does not change in electrophoretic mobility and merely decreases in intensity as the PLL concentration increases with a second band appearing halfway and again remains at constant electrophoretic mobility. This indicates a system where either a $T = 1$ capsid has PLL bound or it has not, and no reversible interaction between the two occurs. At 50 mM of NaCl the linear PLL is most likely bound by the $T = 1$ capsid groove, lying, as it were, flat in the groove at 2 nm depth and not be able to have meaningful interactions with charges on any neighboring capsid due to a Debye screening length of only 1.2 nm. At higher concentrations it could compete with other PLL polymer chains, to weaken interaction and allow for clustering at concentrations greater than 25 µg/ml PLL (2.63 mM) for 50 µg/ml CPSS seen in DLS.

These results indicate a stronger binding between the PLL and $T = 1$ CPSS VLPs compared to the $T = 3$ CCMV VLPS, which should allow the $T = 1$ CPSS VLP to out compete the $T = 3$ CCMV for PLL if both are mixed. To test this hypothesis, competition experiments between the two VLPs were
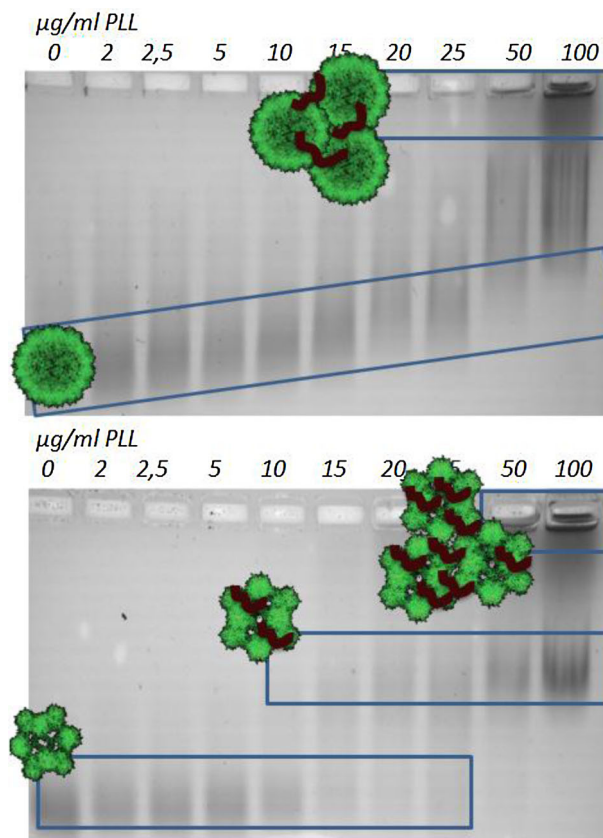

Figure 8. Agarose Gel Electrophoresis of $T = 3$ (top) and $T = 1$ (bottom) of protein cage clusters formed in 50 mM of NaCl at 100 µg/ml of protein and increasing PLL concentration.
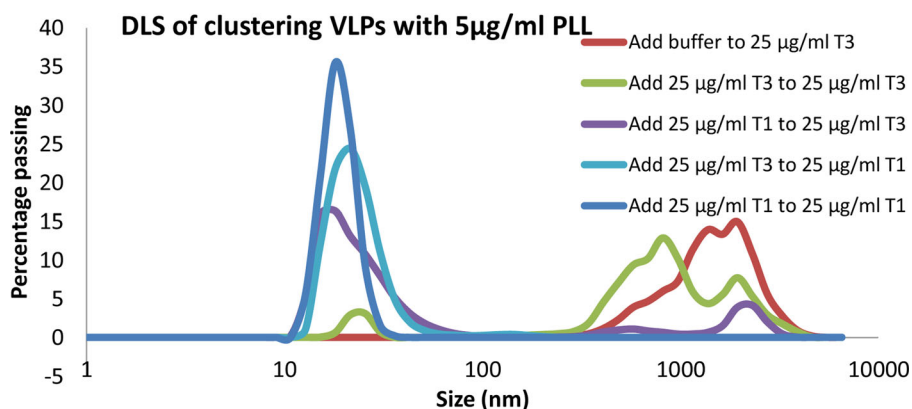
Figure 9. Competition experiments between $T = 3$ CCMV and $T = 1$ CPSS monitored by dynamic light scattering. Starting at 25 µg/ml of protein the sample was subsequently diluted by the addition of a second solution as indicated in the figure above.

carried out, in which equal quantities of VLP protein were mixed in different order at 50 mM of NaCl (Figure 9). Initially, 25 µg/ml of $T = 3$ CCMV and 5 µg/ml of PLL is used to form clusters, upon the addition of either more buffer solution or 25 µg/ml of $T = 3$ CCMV a conservation of clustered particles is observed by DLS. However, upon addition of 25 µg/ml of $T = 1$ CPSS, instead of buffer or $T = 3$ CCMV, there is a loss of most of the clustered state, with a broad peak appearing around 20 nm that indicates a mixture of free $T = 1$ and $T = 3$ particles. Similarly, addition of 25 µm/ml of $T = 3$ to a solution of 25 µg/ml of $T = 1$ CPSS and 5 µg/ml of PLL does not show anything but a broad peak for free particles. A control experiment, the addition of 25 µg/ml of $T = 1$ CPSS to a solution of 25 µg/ml of $T = 1$ CPSS and 5 µg/ml of PLL, also shows a peak for free particles, but distinctly narrower as no $T = 3$ sized particles are present. The loss of a signal for clustered materials indicates a decreased clustering, caused by a scavenging of the available PLL clustering agent by the $T = 1$ capsid.

2.4. The Effect of the Polymer Shape on the Clustering

If indeed there is a binding pocket that traps the linear PLL, a polymer of a different shape might show a different interaction with this pocket. To investigate this, spherical PAMAM-G3 (PG3) dendrimers are used in clustering experiments, as they are an established alternative means of clustering $T = 3$ CCMV capsids.[10b] The overall mass of the PG3 dendrimer ($Mw_{PG3} = 6,909$) is within the range of the PLL ($Mw_{PLL} = 4,000–15,000$) and it has a similar amine to mass ratio resulting in a similar charge density. Furthermore, the diameter of this spherical dendrimer is around 3.3 nm,[c] [20] excluding containment in any surface groove.

─────────────

[c]This diameter is two times the radius derived from the solvent accessible surface area, $R_{SASA} = 16.43$ Å, as computed by Maiti et al.[17]

As evident from the dynamic light scattering data (Figure 10), the dendritic PG3 has a very different interaction with the two different VLP symmetries compared to the linear PLL.

The onset point of clustering with the dendrimer appears to be similar for both the $T = 1$ and $T = $ capsids (Figure 10), at 1 mg/ml of proteins for the $T = 3$ CCMV capsid and 2 mg/ml for the $T = 1$ CPSS capsid. Surprisingly, this indicates an average of 10.4 dendrimers for every $T = 3$ capsid or 7.0 for every $T = 1$ capsid, suggesting that not all binding sites on the capsids are needed to form clusters. The $T = 3$ clustering behavior is similar to studies on cationic gold nanoparticles where only 24 out of a possible 60 electrostatic binding sites were found to be used on a $T = 3$ CCMV capsid, and generally 16 were used in a crystalline assembly.[11a] Kostiainen et al. speculate that steric hindrance and electrostatic repulsion could play an important role in preventing neighboring binding sites from being used. Considering the size of the dendrimer, $R_{SASA} = 1.6$ nm,[20] and the distance between two binding sites, ∼6 nm from the model, two adjacent dendrimers should be separated by ≈3 nm. This is more than the Debye length, $\kappa \approx 1.2$ nm for [NaCl] $= 50$ mM, thus limiting the potential effects of steric hindrance and electrostatic repulsion. Instead, we believe that the clustering is more efficient to due to strong dendrimer-binding site interaction deriving from the PG3 structure.

Interestingly, the electron microscopy images of $T = 3$ CCMV-PG3 clusters (Figure 11) show a clear multi-layered structure, with different domains within the crystals having either face centered cubic (fcc) or hexagonal close packing (hcp) structure. This is unlike the images of PLL based clusters, that, though organized, do not show more than two organized layers and no evidence of organization in the third dimension. Similarly, images of $T = 1$ CPSS-PAMAM G3 show a denser structure compared to those clusters formed with PLL. These findings further point to the important role of the molecular structure of PG3, that
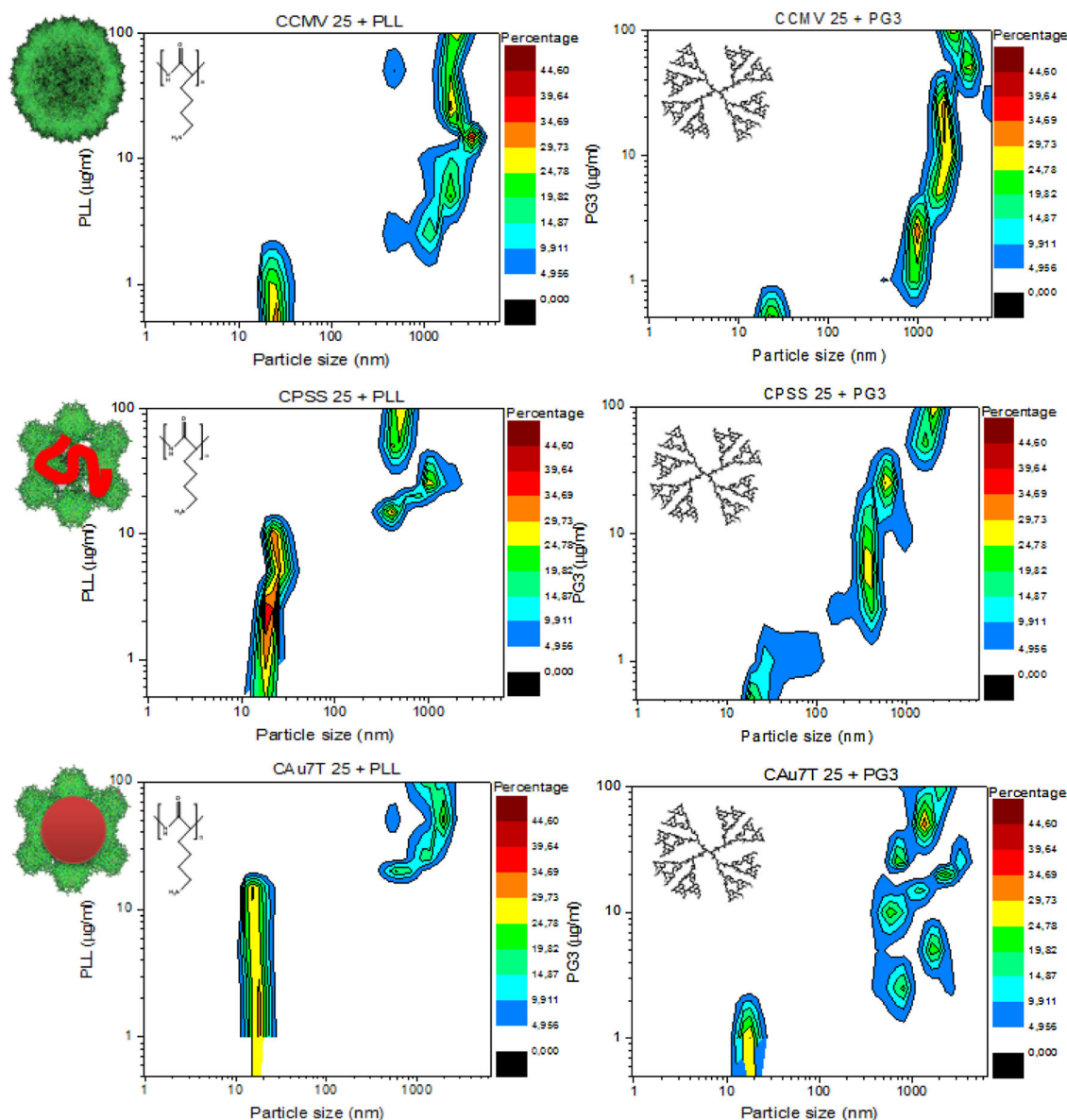
Figure 10. Dynamic light scattering intensity plots at 50 mM NaCl of 25 µg/ml (top) $T = 3$ virus particles (CCMV), (middle) $T = 1$ polymer containing virus capsids (CPSS), and (bottom) gold containing $T = 1$ virus capsids (CAu7T) with increasing PLL concentration (left) and increasing PG3 concentration (right).

apparently prevents the collapse of the structure upon drying. Furthermore, these results can be explained by the symmetrical rotations found in the two different VLPs, with the $T = 3$ having a six-fold, threefold and twofold rotational axis and the $T = 1$ being limited to a fivefold and threefold rotational axis. As the binding sites are arranged according to this symmetry, a $T = 3$ capsid could easily offer a similar binding environment on six symmetrical positions, allowing for hexagonal close packing. The $T = 1$ capsid could only offer a similar binding site on five symmetrical positions thereby limiting it at best to quasi-crystalline

arrangement or topologically close packed (tcp) structure. Such structures are not found and we believe they would require a specifically designed macromolecule, to fine-tune the binding site interaction, combined with carefully control over the clustering conditions, like pH and ionic strength.

2.5. Cargo Independence of Clustering

Ultimately, the goal of this research is to find pathways to organize nanoparticles and other materials contained in the
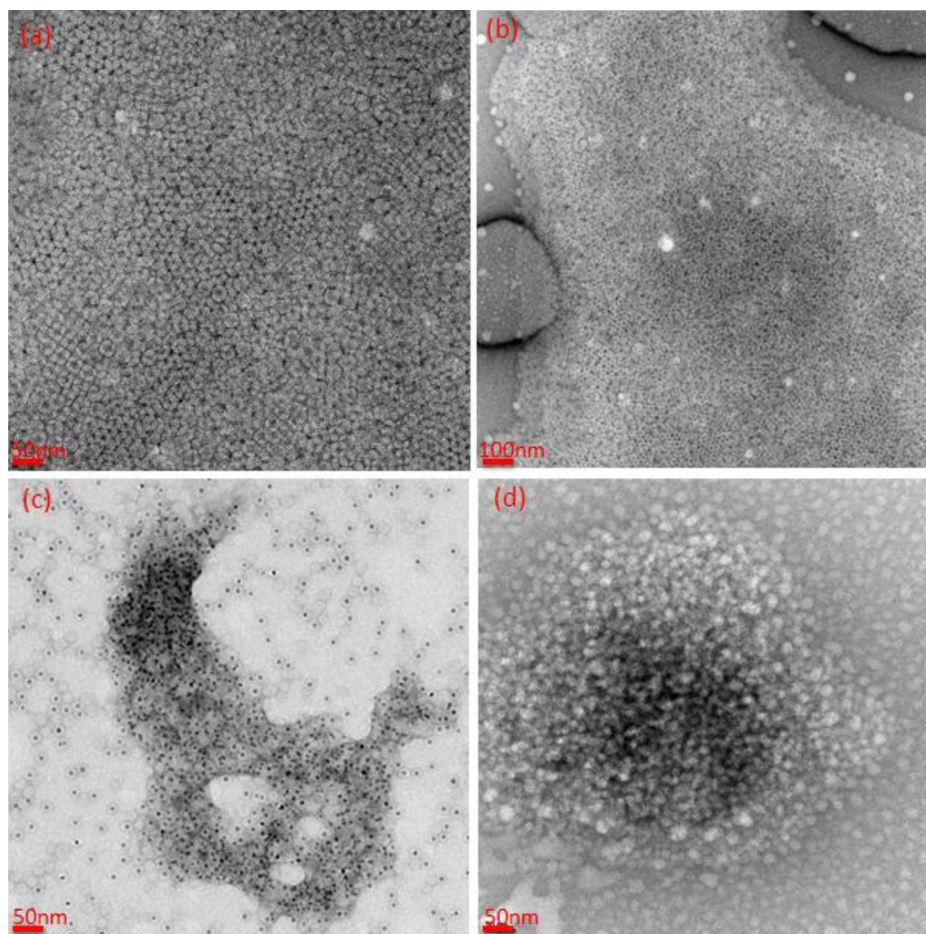
Figure 11. TEM images of 25 µg/ml VLPs clustered with 10 µg/ml of PG3 at 50 mM NaCl. a and b) virus particles (CCMV), c) gold cored $T=1$ virus capsids (CAu7T), and d) polymer cored virus capsids (CPSS).

virus capsids through a uniform method. As such, it is important to show that the clustering depends on the capsid, and thus the symmetry, and not the cargo. To investigate this $T=1$ CAu7T VLPs filled with hard material 7 nm AuNPs, rather than soft PSS or RNA, can be clustered with both PLL and PG3. These particles have been shown to be similar in size and behavior to the $T=1$ VLP, as detailed previously, while the gold plasmon absorption seen in the UV–Vis spectrum (Figure 2), the reduced electrophoretic mobility (Figure 7) and TEM images (Figure 10) of these particles all point to of a dense metallic core.

As expected, the $T=1$ CAu7T VLPs clusters in a similar manner to the $T=1$ CPSS VLPs for both the linear PLL and the spherical PG3 (Figures 10 and 11). The onset point for clustering observed in DLS requires starts at 25 µg/ml of PLL or 2 µg/ml of PG3 for the $T=1$ CAu7T clusters, which is comparable to the results obtained for $T=1$ CPSS, rather than the $T=3$ CCMV. Furthermore, like their soft $T=1$ CPSS counterparts the $T=1$ CAu7T VLPs show little to no organization upon clustering. Investigations on $T=3$ gold

and/or CPSS cored VLPs are, however, desired to confirm if this is due to the capsid symmetry as discussed above or imperfections in the VLP shell formation as is suggested by theoretical work by Nguyen.[21]

3. Conclusion

The size and related symmetry structure, of CCMV based VLPs significantly impacts the electrostatic clustering with soft macromolecules. The nature of the core, whether it is a hard nanoparticle or soft polymer, does not seem to affect cluster formation beyond providing a template for the protein shell. Experimental data, supported by a model of the binding site, suggests that the smaller $T=1$ VLPs will trap linear PLL in a surface groove. This will prevent clustering until the $T=1$ VLP surface is saturated, unlike the $T=3$ VLPs that readily forms clusters with PLL. Clustering with spherical PG3 is, however, similarly efficient for both $T=1$ and $T=3$ VLPs. TEM images show evidence for

organized fcc or hcp structures for the $T = 3$ CCMV VLP clusters, whilst the $T = 1$ VLP clusters show no evidence for organization, which we attribute to the $T = 3$ VLPs' six-fold symmetry axis.

Understanding the differences in clustering between the $T = 1$ and $T = 3$ VLPs enables a more careful control over the desired material properties and structure. As such, the limitations in structural order could be addressed by careful control over both the binding site interaction and conditions, e.g., pH and ionic strength. In fact we believe that by careful tuning of the clustering macromolecules' interaction with the $T = 1$ VLP binding site, quasi-crystalline or tpc structures might be achievable. Additionally, the core independence for $T = 1$ VLP cluster behavior shows the potential universality in forming clusters using the same protein scaffold. Furthermore, even without structural ordering, future studies on these clustered VLP-based materials should also focus on their biological mass transport and biodistribution, as well as their potential toxicity. Collectively, this could open up opportunities for using VLPs as uniform building blocks in new materials for nanomedicine with tuneable imaging, drug delivery and structural properties.

4. Experimental

The following equipment and methods were used to obtain the data in this study.

4.1. Virus and Coat Protein Isolation

CCMV is isolated from infected plant material according to methods adapted from Verduin et al. The CCMV CP is also isolated according to methods developed by Verduin et al. and will be described in brief. CCMV is disassembled into 90 protein dimers by precipitating the RNA using Ca^{2+}, through dialysis against a pH 7.5 aqueous buffered solution (500 mM $CaCl_2$, 50 mM Tris). The RNA-Ca^{2+} precipitate can be pelleted by ultracentrifugation (2 h at 40 000 rpm in Fiberlite F50L$^-$24 × 1.5 rotor) and the remaining Ca^{2+} is subsequently removed by dialysis against the pH 7.5 aqueous buffered solution (50 mM Tris; 500 mM NaCl) yielding a CCMV protein dimer solution.[16]

4.2. CPSS VLP formation

The efficient formation of $T = 1$ capsids using PSS (polystyrene-sulfonate), as described by Sikkema et al., requires a precise ratio between polymer and protein, such that for each protein monomer 40 sulfonate groups are available. In a typical experiment 70 kDa PSS is encapsulated by adding a solution of PSS (milliQ, 2.75 mg/ml, 200 μl) to a room temperature solution of the protein dimers (6 mg/ml, 300 μl). After incubating it on a roller bank for 30 min the resulting VLPs were purified using preparative FPLC using a 0.3 M aqueous buffered solution as the eluent (50 mM Tris; 300 mM NaCl).[15]

4.3. CAu7T VLP Formation

Encapsulation of gold nanoparticles (AuNPs) requires a large excess of protein and precise control over salt concentration to prevent particle aggregation from charge screening whilst maintaining the proteins structure. 7 nm AuNP are encapsulated by adding a room temperature solution of the protein dimers (6 mg/ml, 120 μl) to a solution of AuNPs (milliQ, 0.5 mg/ml, 480 μl) and mixed by vigorous shaking for 15 s. The resulting VLPs were dialyzed overnight against a pH 7.5 aqueous buffered solution (50 mM Tris; 500 mM NaCl) and purified using preparative fast protein liquid chromatography (FPLC).

4.4. Clustering Procedure

Sample solutions are prepared fresh from 1 mg/ml VLP stock solutions in 0 or 50 mM NaCl cluster buffer solution (10 mM sodium acetate, 1 mM EDTA, 1 mM NaN_3, pH 5.0) and 1 mg/ml of polymer stock solution in milliQ, either PLL or PG3. First, an aliquot of the VLP stock solution is diluted by addition of further cluster buffer solution. Then, the ionic strength is adjusted by addition of 1 M NaCl cluster buffer. Finally a small volume of the polymer is added such that the final concentrations are as desired.

4.5. Agarose

A 1.2% w/v agarose gel is cast in a low salt-buffered solution (50 mM NaCl, 10 mM sodium acetate, 1 mM EDTA, 1 mM NaN_3) and allowed to solidify for 30 min and subsequently immersed in a similar buffer. Samples are taken from 50 μl of freshly made sample solution allowed that are left to equilibrate into clustered or unclustered states for 10 min on a shaking platform or roller bank after mixing. The samples are injected into 50 μl sample wells and left to run for 2 h at a potential difference of 100V. Afterwards samples are stained for 2 h using bio safe coomassie blue and washed three times for at least 2 h using milliQ to remove excess staining.

4.6. Transmission Electron Microscopy

Samples are taken from 100 μl of freshly made sample solution allowed that are left to equilibrate into clustered or unclustered states for 10 min on a shaking platform or roller bank after mixing. The TEM samples are prepared by leaving 5 μl of this sample solution on a formvar carbon coated copper grid for 5 min and subsequently removing it by tipping the grid onto low lint paper (Kimtech science precision wipes). Stained samples use 5 μl of a 1% Uranyl Acetate solution, which is removed after 30 s to provide optimal contrast. Samples are imaged using a Philips CM300ST-FEG TEM.

4.7. DLS

Dynamic light scattering samples are prepared from 500 μl fresh sample solutions and allowed to equilibrate for 2 min on a roller bank after mixing. Salt concentrations were controlled by using stock solutions of 0 and 1 M NaCl containing buffers and in all cases the cationic polymer was the final addition. Each sample was

Materials
Views
www.MaterialsViews.com

Macromol. Biosci. **2015,** *15,* 98–110
© 2014 WILEY-VCH Verlag GmbH & Co. KGaA, Weinheim

Macromolecular
Journals

109

measured five times for 120 s using an Anaspec nanotrack wave dynamic light scattering instrument with the best of these five measurements selected.

4.8. UV–Visible

UV–Visible samples are prepared from 500 μl fresh sample solutions and allowed to equilibrate for 2 min on a roller bank after mixing. They were measured in a 1 cm quartz cuvette in a PerkinElmer Lambda 850 UV/VIS Spectrometer.

4.9. FPLC

FPLC size exclusion chromatography samples, ranging from 100 μl up to 500 μl were measured on a 24 ml column stacked with superose-6 and collected by fractionation.

4.10. Materials

CCMV was isolated in our own lab. 7 nm AuNPs were obtained from nanoComposix as 7 nm Tannic NanoXact Gold Nanospheres. All other chemicals were purchased from Sigma Aldrich at bioreagent grade or similar purity.

[1] a) T. L. Doane, C. Burda, *Chem. Soc. Rev.* **2012**, *41*, 2885; b) Y. Ma, R. J. M. Nolte, J. J. M. Cornelissen, *Adv. Drug Deliv. Rev.* **2012**, *64*, 811.

[2] X.-Q. Zhang, X. Xu, N. Bertrand, E. Pridgen, A. Swami, O. C. Farokhzad, *Adv. Drug Deliv. Rev.* **2012**, *64*, 1363.

[3] L. Xu, W. Ma, L. Wang, C. Xu, H. Kuang, N. A. Kotov, *Chem. Soc. Rev.* **2013**, *42*, 3114.

[4] F. Li, Q. Wang, *Small* **2014**, *10*, 230.

[5] a) S. Kang, P. A. Suci, C. C. Broomell, K. Iwahori, M. Kobayashi, I. Yamashita, M. Young, T. Douglas, *Nano Lett.* **2009**, *9*, 2360; b) F. Li, H. Chen, L. Ma, K. Zhou, Z.-P. Zhang, C. Meng, X.-E. Zhang, Q. Wang, *Small* **2014**, *10*, 536.

[6] a) J. A. Speir, S. Munshi, G. Wang, T. S. Baker, J. E. Johnson, *Structure* **1995**, *3*, 63; b) L. Loo, R. H. Guenther, V. R. Basnayake, S. A. Lommel, S. Franzen, *J. Am. Chem. Soc.* **2006**, *128*, 4502.

[7] F. Li, D. Gao, X. Zhai, Y. Chen, T. Fu, D. Wu, Z.-P. Zhang, X.-E. Zhang, Q. Wang, *Angew. Chem. Int. Ed.* **2011**, *50*, 4202.

[8] a) N. F. Steinmetz, G. Calder, G. P. Lomonossoff, D. J. Evans, *Langmuir* **2006**, *22*, 10032; b) N. F. Steinmetz, E. Bock, R. P. Richter, J. P. Spatz, G. P. Lomonossoff, D. J. Evans, *Biomacromolecules* **2008**, *9*, 456.

[9] a) P. J. Yoo, K. T. Nam, J. F. Qi, S. K. Lee, J. Park, A. M. Belcher, P. T. Hammond, *Nat. Mater.* **2006**, *5*, 234; b) P. A. Suci, M. T. Klem, T. Douglas, M. Young, *Langmuir* **2005**, *21*, 8686; c) N. F. Steinmetz, K. C. Findlay, T. R. Noel, R. Parker, G. R. Lomonossoff, D. J. Evans, *ChemBioChem* **2008**, *9*, 1662.

[10] a) M. A. Kostiainen, O. Kasyutich, J. Cornelissen, R. J. M. Nolte, *Nat. Chem.* **2010**, *2*, 394; b) M. A. Kostiainen, P. Hiekkataipale, J. A. de la Torre, R. J. M. Nolte, J. J. L. M. Cornelissen, *J. Mater. Chem.* **2011**, *21*, 2112.

[11] a) M. A. Kostiainen, P. Hiekkataipale, A. Laiho, V. Lemieux, J. Seitsonen, J. Ruokolainen, P. Ceci, *Nat. Nano* **2013**, *8*, 52; b) A. L. Bozic, R. Podgornik, *J. Chem. Phys.* **2013**, 138.

[12] D. L. D. Caspar, A. Klug, *Cold Spring Harbor Symp. Quant. Biol.* **1962**, *27*, 21.

[13] J. Sun, C. DuFort, M.-C. Daniel, A. Murali, C. Chen, K. Gopinath, B. Stein, M. De, V. M. Rotello, A. Holzenburg, C. C. Kao, B. Dragnea, *Proc. Natl. Acad. Sci.* **2007**, *104*, 1354.

[14] M. A. Kostiainen, C. Pietsch, R. Hoogenboom, R. J. M. Nolte, J. Cornelissen, *Adv. Funct. Mater.* **2011**, *21*, 2012.

[15] F. D. Sikkema, M. Comellas-Aragones, R. G. Fokkink, B. J. M. Verduin, J. J. L. M. Cornelissen, R. J. M. Nolte, *Org. Biomol. Chem.* **2007**, *5*, 54.

[16] B. Verduin, *FEBS Lett.* **1974**, *45*, 50.

[17] M. Comellas-Aragones, *The Cowpea Chlorotic Mottle Virus as a Building Block in Nanotechnology*, UB Nijmegen [Host], **2009**.

[18] X. Liu, M. Atwater, J. Wang, Q. Huo, *Colloids Surf. B: Biointerfaces* **2007**, *58*, 3.

[19] J. Lyklema, *Fundamentals Of Interface And Colloid Science, Volume 5: Soft Colloids*, Vol. 5, Academic Press. **2005**.

[20] P. K. Maiti, T. Çan, G. Wang, W. A. Goddard, *Macromolecules* **2004**, *37*, 6236.

[21] H. D. Nguyen, C. L. Brooks, *Nano Lett.* **2008**, *8*, 4574.